THE TIME-DEPENDENT HARTREE-FOCK DESCRIPTION OF HEAVY-ION COLLISIONS: A PROGRESS REPORT

S. J. Krieger
University of California, Lawrence Livermore National Laboratory
Livermore, California 94550 U.S.A.

1. INTRODUCTION

Although the time-dependent Hartree-Fock (TDHF) approximation was formulated by Dirac[1] over 50 years ago, it is only in the last six years that TDHF calculations have actually been effected. The initial application of the TDHF approximation, by Bonche, Koonin, and Negele[2], to reactions between semi-infinite slabs of nuclear matter produced a rich collision phenomenology which included compound "nucleus" formation, resonances, and highly inelastic reactions. In this seminal calculation, the dynamics were conspicuously dominated by the propagation and reflection of single-particle wave functions in the mean HF potential. Indeed, much of the work in the past several years has been devoted to the question as to what extent the single-particle dynamics and collision phenomenology would persist in more realistic calculations, and it is only recently that emphasis has shifted to comparison of TDHF results with experiment. Prior to discussing these results of the greater part of a decade of research, however, it is useful to review the motivations for applying the TDHF approximation to nuclei.

The ultimate goal of any microscopic theory of nuclear motion is to provide a unified description of the reaction dynamics for such diverse physical phenomena as giant multipole resonances, fission, fusion, and compound nucleus formation. TDHF is indeed a candidate for such a microscopic theory, since it requires as input only an effective nuclear interaction, and the specification of initial conditions. No assumptions need be made as to the relevant collective or intrinsic coordinates. Also, TDHF offers an additional bonus. Because TDHF is a quantal independent particle approximation, it admits to a semiclassical interpretation, thus offering possible insight into the underlying physics, which would not be obtainable in calculations using more complicated wave functions. This bonus, however, is not without cost. Given the physical picture of independent nucleons moving in their self-generated, time-dependent one-body potential, it is clear that the approximation can only be valid at energies below that in which the dominant interaction is that of nucleon-nucleon collisions. At first sight this limitation on the domain of applicability of the theory might appear to severely restrict its usefulness. For unlike the static HF approximation which has been so successful over the past two decades in calculating the properties of the ground states and low-lying excited states of nuclei throughout the periodic table, the

*Work performed under the auspices of the U. S. Department of Energy by the Lawrence Livermore National Laboratory under contract No. W-7405-ENG-48.

TDHF approximation is used in situations in which the same strongly interacting fermion systems are far from equilibrium. Fortunately the regime in which the approximation may be applied need not be so severely limited. For although the mean free path for a nucleon at high energies, $E/A >> \epsilon_F$, is indeed only a small fraction of the nuclear diameter, at energies of but a few MeV per nucleon above the Coulomb barrier the suppression of the number of accessible final states due to the Pauli principle insures that at such low energies, $E/A << \epsilon_F$, the mean free path is several times greater than the nuclear size.[3] To iterate, even though the applications of interest deal with strongly interacting systems, far from equilibrium, the Pauli blocking is nevertheless effective enough to render the independent-particle TDHF theory a reasonable first approximation to the solution of such problems.

Having motivated the use of TDHF in studying the processes observed in heavy ion collisions, it is perhaps useful to comment on some of the other methods, such as resonating groups,[4] generator coordinates,[5] the random phase approximation (RPA),[6] adiabatic time-dependent Hartree-Fock,[7] and fluid dynamics[8] which have previously been employed to describe these processes. As we shall see, none of these methods is without its drawbacks. Thus, computational complexities restrict the application of the resonating group method to all but the lightest nuclei, while in the case of generator coordinates it is necessary, in order to make calculations feasible, to select, a priori, the allowed collective degrees of freedom. The RPA, being a linearized version of TDHF, is applicable only to small amplitude disturbances, and ATDHF is limited to the description of low-lying excitations in the case of large amplitude motion,[9] and may even be further limited.[10] Finally the application of fluid dynamics to nuclei depends upon approximations whose validity can be determined only by testing them by a more complete microscopic theory.[11]

Information concerning the question as to whether the TDHF approximation indeed yields the correct mean field theory is now being generated by a number of works,[12),13)] treating the time-dependent mean field problem. These works,[12),13)] which seek both to offer a rigorous justification of the TDHF method, as well as to overcome some of the serious conceptual and practical problems[14] inherent in the method, are making it increasingly plausible that TDHF is the correct mean field theory for the calculation of one-body observables.

Such conformation is indeed important. For while the TDHF equations can be derived from a time-dependent variational principle,[15] there is an important conceptual difference in its application as compared to the principle which gives rise to the static HF equations. In the static case it is known that one obtains the best wave function in the sense that the solution of the HF equations yields the determinant in which the expectation value of the energy is closest to the exact energy. While the above does not insure that the wave functions necessarily will yield accurate values of other observables, it nevertheless is a stronger statement than one can make in the dynamic situation. Perhaps the best that can

be done in the latter case is to show that if, at any time, the exact wave function is a Slater determinant, then the TDHF wave function yields the Slater determinant which maximizes the overlap with the exact wave function in the interval about that time.[16]

Given the theoretical difficulties in establishing the validity of the TDHF approximation, it is perhaps most effective at this time to assess the results of the TDHF calculations by comparing them, insofar as is possible, with experimental results. In this task we shall be limited by the fact that the TDHF approximation does not yield an inclusive description of nuclear reactions, but rather an exclusive description of nuclear collisions.[13] Thus the semi-classical nature of the approximation which offers such a simple picture of certain gross properties, at the same time effectively prohibits the acquisition of detailed channel information. In spite of this we shall still succeed in showing rather good agreement between theory and experiment for the particular reactions which result in fusion or in deep inelastic collisions. For a more complete (and more balanced) review of TDHF results the reader is referred to four recent review articles.[17]

The structure of this review is as follows. In Section 2 the TDHF equations are derived and briefly discussed. The effective interaction employed in the calculations is described in Section 3, and some technical aspects of the calculations are discussed in Section 4. Fusion results are presented in Section 5 along with a brief discussion of deep inelastic collisions. Finally, the results are summarized in Section 6.

2. THE TDHF EQUATIONS

The TDHF equations may be derived from a variational principle[15] which bears a formal resemblance to the stationary action principle which gives rise to the time-dependent many-body Schrödinger equation. To be specific, the TDHF equations follow from the requirement

$$\delta \int dt\, \Psi^{\dagger} \left(i\hbar \frac{\partial}{\partial t} - H\right) \Psi = 0 \tag{2.1}$$

where H is the full many-body Hamiltonian, but Ψ, the many-body wave function, is restricted at all times to the subspace of Slater determinants. In the coordinate representation, with this restriction on Ψ (and with spin and isospin labels suppressed), the linear Schrödinger equation for the A particle system is replaced by A coupled, non-linear differential equations for the A occupied orbitals $\psi_i(\mathbf{r},t)$

$$i\hbar \frac{\partial}{\partial t} \psi_i(\mathbf{r},t) = \frac{\delta \langle \Psi | H | \Psi \rangle}{\delta \psi_i^*(\mathbf{r},t)} \qquad i = 1,2,\ldots A \tag{2.2}$$

Equations (2.2) conserve in time a number of important quantities including the expectation value of the energy, H, the total momentum, the total angular momentum, and the scalar products of the single-particle wave functions, $\langle \psi_i | \psi_j \rangle = \delta_{ij}$. Insight into the underlying physics governed by equations (2.2) can be obtained by considering the situation in which the Hamiltonian, H, consists of the kinetic energy plus a local central two-body potential, V(r). In this case the energy functional

$$\langle \Psi | H | \Psi \rangle = \int d^3r\, \frac{\hbar^2}{2m} \tau(\mathbf{r},t) + \frac{1}{2} \int d^3r\, d^3r'\, \rho(\mathbf{r},t)\, V(\mathbf{r}-\mathbf{r}')\, \rho(\mathbf{r}',t)$$

$$- \frac{1}{2} \int d^3r\, d^3r'\, |\rho(\mathbf{r},\mathbf{r}',t)|^2\, V(\mathbf{r}-\mathbf{r}') \,, \tag{2.3}$$

where $\rho(\mathbf{r},\mathbf{r}',t) = \sum_{i=1}^{A} \psi_i(\mathbf{r},t)\, \psi_i^*(\mathbf{r}',t)$ is the one-body density matrix, whose diagonal elements yield the particle density $\rho(\mathbf{r},t) \equiv \rho(\mathbf{r},\mathbf{r},t)$, and $\tau(\mathbf{r},t) = \nabla_{\mathbf{r}} \cdot \nabla_{\mathbf{r}'} \rho(\mathbf{r},\mathbf{r}',t)|_{\mathbf{r}=\mathbf{r}'}$ is the kinetic energy density. Variation of equation (2.3) as called for by equations (2.2) then results in the TDHF equations

$$i\hbar \frac{\partial}{\partial t} \psi_i(\mathbf{r},t) = -\frac{\hbar^2}{2m} \nabla^2 \psi_i(\mathbf{r},t) + \int d^3r'\, V(\mathbf{r}-\mathbf{r}')\, \rho(\mathbf{r}',t)\, \psi_i(\mathbf{r},t)$$

$$- \int d^3r'\, V(\mathbf{r}-\mathbf{r}')\, \rho(\mathbf{r},\mathbf{r}',t)\, \psi_i(\mathbf{r}',t) \,. \tag{2.4}$$

Neglecting for the moment the third term on the right of equation (2.4), it may be noted that each single-particle wave function simply evolves through a Schrödinger equation in which the potential is given by the mean field generated by the instantaneous nuclear density. The third term then gives the exchange term required by the Pauli principle.

3. THE EFFECTIVE INTERACTION

Although calculations have been effected using a realistic phenomenological K-matrix model[18] for head-on collisions of $^{12}C + {}^{12}C$, these calculations are technically complicated, and have neither been extended to collisions at finite impact parameters nor to collisions of heavier ions. In this review we shall therefore discuss calculations which have been effected using effective interactions of the Skyrme type.[19] Skyrme's interaction[19] consists of a two-body term $V^{(2)}$ including a spin-orbit potential, and a three-body term $V^{(3)}$. In the coordinate representation, $V^{(2)}$ and $V^{(3)}$ are expressed as

$$V^{(2)}(\mathbf{r}_1,\mathbf{r}_2) = t_0(1+x_0P_\sigma)\,\delta(\mathbf{r}_1-\mathbf{r}_2) + \tfrac{1}{2}\,t_1[\delta(\mathbf{r}_1-\mathbf{r}_2)\,k^2 + k'^2\,\delta(\mathbf{r}_1-\mathbf{r}_2)]$$

$$+ t_2\,\mathbf{k}'\cdot\delta(\mathbf{r}_1-\mathbf{r}_2)\mathbf{k} + iV_{s.o.}(\sigma_1+\sigma_2)\cdot\mathbf{k}'\times\delta(\mathbf{r}_1-\mathbf{r}_2)\,\mathbf{k}\,, \qquad (3.1)$$

$$V^{(3)}(\mathbf{r}_1,\mathbf{r}_2,\mathbf{r}_3) = t_3\,\delta(\mathbf{r}_1-\mathbf{r}_2)\,\delta(\mathbf{r}_2-\mathbf{r}_3)\,. \qquad (3.2)$$

In equation (3.1) P_σ is the spin exchange operator and σ represents the vector of the Pauli spin matrices; $\mathbf{k}$ is the operator $\frac{1}{2i}(\nabla_1-\nabla_2)$ acting on the right and $\mathbf{k}'$ is $-\frac{1}{2i}(\nabla_1-\nabla_2)$ acting on the left. The quantities x_0, t_0, t_1, t_2, t_3 and the spin-orbit coupling strength $V_{s.o.}$ are parameters of the specific Skyrme interaction. A particular virtue of the zero-range nature of the interaction is that the expectation value of the many-body Hamiltonian can simply be written as an integral of an energy density $H(\mathbf{r})$,

$$\langle\Psi|H|\Psi\rangle = \int d^3r\, H(\mathbf{r}) \qquad (3.3)$$

which itself depends only upon various special densities which can be constructed from the single-particle density matrix. Full details are given in reference 9. However, in the special case of a spin-saturated and charge conjugated nucleus, the energy density reduces to

$$H(\mathbf{r}) = \frac{\hbar^2}{2m}\tau + \frac{3}{8}t_0\rho^2 + \frac{1}{16}(3t_1+5t_2)(\rho\tau-\mathbf{j}^2) - \frac{1}{64}(9t_1-5t_2)\,\rho\,\nabla^2\rho$$

$$+ \frac{1}{16}t_3\rho^3 \qquad (3.4)$$

In equation (3.4) $\mathbf{j}$ is the momentum density

$$\mathbf{j}(\mathbf{r},t) = \frac{1}{2i}[(\nabla-\nabla')\,\rho(\mathbf{r},\mathbf{r}',t)]_{\mathbf{r}=\mathbf{r}'}\,. \qquad (3.5)$$

In this case the TDHF equations are extremely simple. The Hamiltonian, $h(\mathbf{r})$, governing the time evolution of the single-particle wave functions then takes the form[9]

$$h(\mathbf{r}) = -\nabla\cdot\left[\frac{\hbar^2}{2m^*(\mathbf{r})}\nabla\right] + U(\mathbf{r}) + \frac{1}{2i}[\nabla\cdot I(\mathbf{r}) + I(\mathbf{r})\cdot\nabla]\,. \qquad (3.6)$$

In equation 3.6, $m^*(\mathbf{r})$ is an effective mass whose inverse is linearly proportional to the density, $U(\mathbf{r})$ is a potential linearly proportional to the density and kinetic energy density, and $I(\mathbf{r})$ is linearly proportional to the momentum density. Thus, by using the Skyrme interaction, the generally non-local HF Hamiltonian is reduced to a second order differential operator, and the numerical solution of the TDHF equations is thereby not only significantly eased, but made considerably faster.

The use of the Skyrme interactions in TDHF calculations is motivated not only by the resulting computational facility outlined above, but also by the fact that the interactions have been utilized in static HF calculations to give an excellent description of nuclear ground state properties for a broad range of nuclei throughout the periodic table.[20] Finally, while the Skyrme interaction has been introduced strictly as a phenomenological effective interaction, its form can be justified theoretically by the density matrix expansion[21] and density-dependent HF approach.[22]

For completeness we should note that in some of the calculations to be discussed, the surface energy term proportional to $\nabla^2\rho$ in equation 3.4 has been replaced for numerical reasons by a double convolution of the density with a short-range Yukawa interaction. In such cases the parameters t_0 and x_0 are renormalized as the double convolution of the density also contributes a term proportional to ρ^2.[23] Though we did not so indicate, the direct Coulomb contribution to the energy has been included in the calculations. Inclusion of the Coulomb exchange term, in the local Slater approximation, has been shown to have no effect on the dynamics of the relatively light $^{40}Ca + {}^{40}Ca$ system.[24] For reasons of computational efficiency, none of the calculations to be reviewed have utilized the spin-orbit term in the interaction. However, recent improvements in the algorithm for calculating the orbital angular momentum suggest the possibility of including this term in future calculations.[25]

4. METHOD OF CALCULATION

A. Description of Models

Although technological advances have made possible the solution of the TDHF equations in full three-dimensional geometry, such calculations are extremely time-consuming, and it is therefore desirable, where possible, to reduce the number of non-trivial spatial dimensions from three to two. For this reason, as well as for the reason that almost all calculations effected to date have utilized a two-dimensional geometry, we shall review the various two-dimensional models and comment upon the regime in which they are expected to yield good approximations to the exact three-dimensional geometry. We shall restrict our discussion to coordinate space models since models which introduce[26] deformed oscillator bases are limited to light systems because of the large number of basis states required to achieve convergence.

In the clutching model[27] the assumption is made that the colliding nuclei retain axial symmetry about the (rotating) line joining their respective centers. In this model the single-particle wave functions are assumed to be of the form

$$\psi_i(\mathbf{r}) = \psi_i(r,z)\, e^{i|\mu_i|\phi} . \tag{4.1}$$

As in the case of the ordinary Schrödinger equation with axial symmetry, the dependence upon ϕ is eliminated upon substitution of the wave function into the equations of motion, and the desired goal of reducing the problem to one involving two non-trivial spatial dimensions, in this case r and z, has been achieved. In order to acount for the energy of rotation of the body fixed axis, the energy functional is supplemented through the addition of the classical rotational energy

$$H \to H + \frac{L^2}{2I(\rho)} , \tag{4.2}$$

where L is the conserved total angular momentum along the axis of rotation which is perpendicular to the reaction plane, and the moment of inertia $I(\rho)$ is a prescribed function of the density. Initially, when the colliding ions are well separated, the moment of inertia is assumed to be that of two point masses. However, when the minimum density along the symmetry axis between the two ions exceeds a value arbitrarily taken to be one-half the saturation density of nuclear matter, the ions are assumed to have clutched and the moment of inertia is then taken to be that of a rigid body. Other prescriptions for the moment of inertia have been studied[28] as well. In this model the symmetry axis is assumed to rotate in space with the classical angular frequency

$$\omega = \frac{L}{I(\rho)} \tag{4.3}$$

and Coriolis forces are completely omitted.

Some of the arbitrariness in the clutching model is removed by multiplying the wave functions, equations 4.1, by the function $e^{i\chi_i(r,z,\phi)}$.[28),29)] With the introduction of the additional phase χ, the model is completely self-consistent with all quantities derivable from the variational principle. Thus no assumption as to the nature of the rotational energy (as in equation 4.2) need be made, and the moment of inertia arises naturally, again without requiring assumptions as to its form.

Unfortunately if the χ_i for the single-particle wave functions are allowed to differ, the resulting equations are then almost as complicated to solve as the full three-dimensional equations. On the other hand, when the same χ, taken to be

$$\chi(r,z,\phi) = g(r,z)\cos\phi \ , \tag{4.4}$$

is used for each wave function, the χ term in the velocity field corresponding to these wave functions is irrotational and therefore cannot describe the physically expected rigid body motion.

The separable approximation[30),31)] is motivated by the fact that in collisions described by the TDHF approximation very little momentum is transferred in the z-direction perpendicular to the reaction plane. Guided by this observation one separates each single-particle wave function into a time-dependent function ϕ_i of the coordinates in the reaction plane and a time independent function χ_i

$$\psi_i(\mathbf{r},t) = \phi_i(x,y,t)\ \chi_i(z) \ . \tag{4.5}$$

The functions χ_i are chosen once and for all at time t = 0 as the appropriate harmonic oscillator wave functions. In the case of mass asymmetric systms, the appropriate oscillator parameter for the wave functions may be chosen, for example, to be that which minimizes the combined energy of the two non-interacting ions. The two non-trivial coordinates in this model are clearly the cartesian coordinates in the reaction plane. In contrast to the clutching models which impose axial symmetry in the rotating frame, the separable approximation makes no such restriction and non-axial configurations are allowed.

B. Accuracy of Models

For closed shell nuclei the axially symmetric calculations are in exact agreement with three-dimensional calculations for head-on collisions. (In open shell nuclei, small deviations can occur due to the different filling prescriptions[32)] employed in the distinct geometries.) Thus the results of calculations employing the axially-symmetric codes will necessarily agree with the results using the three-dimensional codes for small values of the angular momentum, in the vicinity of the L = 0 head-on collisions, as well as for grazing collisions in which the ions interact only weakly.

In order to assess the accuracy of the axially symmetric approximation for

other values of the angular momentum, it is instructive to examine Figure 4.1,

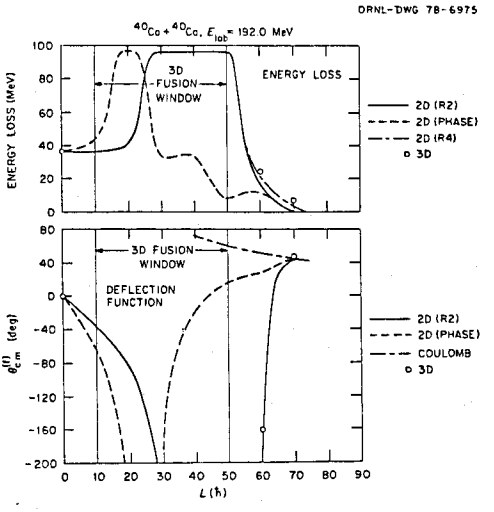

Figure 4.1 Energy loss and deflection function. The full curve is for the clutching model, the dashed for the phase model and the open circles for three dimensional results.[28]

which displays the energy loss and deflection functions curves for $^{40}Ca + ^{40}Ca$, calculated[28] using various axially symmetric models, as well as the three-dimensional code, at the laboratory energy of 192 MeV. At this energy, the three-dimensional code predicts that the colliding ions will fuse when the total angular momentum, L, is in the region $10\hbar \lesssim L \lesssim 50\hbar$. The results of calculations using the clutching model are in reasonably good agreement, predicting fusion in the region $30\hbar \lesssim L \lesssim 50\hbar$. However the phase theory predicts fusion only in a very narrow range of L values centered about $L \sim 20\hbar$. Although it is by no means obvious from this limited comparison, this figure does illustrate a behavior which has been generally observed. Namely the phase theory best reproduces the three-dimensional results at the lower end of the fusion region, while the clutching model more accurately reproduces the results at the upper part of the region. From this behavior it can be inferred that the moment of inertia is essentially irrotational for low values of L, but becomes predominantly rigid body in nature for high values of the angular momentum.

At higher energies and especially in collisions of highly mass asymmetric systems, non-axial deformations become increasingly more important, and the axial approximations break down. For example at a laboratory energy of 278 MeV, three-dimensional calculations of $^{40}Ca + ^{40}Ca$ result in fusion for $25\hbar \lesssim L \lesssim 70\hbar$, while the clutching model exhibits but a narrow orbiting region and no fusion whatsoever. The conclusion is that the clutching model can usefully be employed for head-on collisions, but in the case of collisions at finite impact parameter must be

restricted to calculations at energies not much higher than the interaction barrier.

The separable approximation has successfully reproduced the results of the three-dimensional calculations much more closely than the axial symmetric models over a wide range of energies.[31] This accuracy is illustrated in Figure 4.2 in

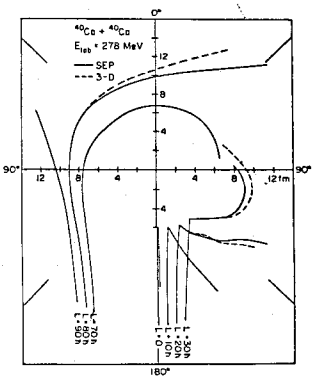

Figure 4.2 Comparison of trajectories calculated in the separable approximation (full curves) with three dimensional results (dashed).[31]

which trajectories are compared for several values of the angular momentum for $^{40}Ca + ^{40}Ca$ at a laboratory energy of 278 MeV.[31] Except for the minor differences observed at $L = 20\hbar$ and $L = 30\hbar$, and the difference at $L = 80\hbar$, where the test is perhaps unreasonably strict as the scattering angle changes extremely rapidly in this orbiting region, the results of the separable approximation are indistinguishable from the three-dimensional results. Similar agreement is obtained in comparing the deflection function and energy loss curves at this energy. Moreover, whereas the clutching model gives no fusion at this energy, the separable approximation results in fusion for the same values of angular momentum as the three-dimensional calculation. In Figure 4.3 the fragment separation coordinate, defined as in

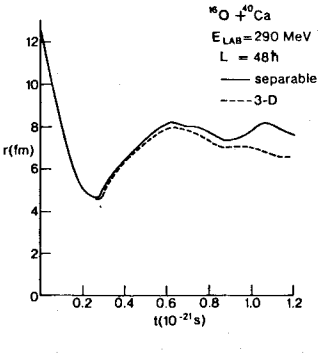

Figure 4.3 Comparison as a function of time of the fragment separation coordinate as calculated in the separable approximation and three dimensions.[45]

reference 27, is plotted as a function of time in a collision between ^{16}O and ^{40}Ca ions at a laboratory energy of 290 MeV with $L = 48\hbar$. The separable approximation yields results in excellent agreement with the results of the fully three-dimensional calculation, until $t \approx 9 \times 10^{-22}$s, by which time the system has fused.

Although the separable approximation has been shown to yield excellent results over a wide range of energies, further tests of the approximation are still required. For some recent calculations for the highly mass asymmetric system $^{16}O + ^{93}Nb$ indicate discrepancies between the separable and axially symmetric models for the case of head-on collisions.[33]

5. RESULTS

Fusion cross-sections cannot be extracted with total unambiguity from either the experimental data or from the results of TDHF calculations. Experimentally, the fusion cross section is defined as the cross-section for observing a composite system with mass close to that of the total mass of the system. For light systems at low bombarding energies the compound nucleus so formed decays almost entirely by light particle and γ-ray emission, so that the fusion cross section is in fact equal to the evaporation residue cross section.[34] At the other end of the spectrum, for heavy systems, A > 200, the dominant decay mode of the compound system is fission, and the fusion cross section can be equated to the cross section for the observation of fusion-fission events. The latter, at least in the case of highly asymmetric collisions, can be distinguished from deep inelastic events by the symmetric mass distribution, as the compound system exists for a sufficiently long time to allow mass equilibration.[35]

In the TDHF calculations it is practical only to follow the composite system through a few rotations, or, in the case of axially symmetric calculations, through a few oscillations of its rms radius. The assumption is then implicitly made that by this time the system no longer retains a memory of the entrance channel, and it is therefore meaningful to compare the cross section for such events with the evaporation residue cross section for light systems, and the fusion-fission cross section for heavy systems. Note too that if this argument is accepted, then the question as to the accuracy with which TDHF can describe the long-time behavior of the system is no longer pertinent to the calculation of fusion cross sections.

The TDHF fusion cross section is calculated at a given energy by determining the minimum and maximum values of angular momentum, $\ell_< \hbar$ and $\ell_> \hbar$ respectively, for which the system fuses and then using the sharp cut-off approximation[36]

$$\sigma_f = \frac{\pi}{k^2} \sum_{\ell_<}^{\ell_>} (2\ell + 1)$$

$$= \frac{\pi\hbar^2}{2\mu E_{cm}} [(\ell_> + 1)^2 - (\ell_< + 1)^2] . \qquad (5.1)$$

In the above, k is the relative wave-vector of the colliding ions, and E_{cm} the center of mass energy. Note that if the TDHF approximation yields fusion for the same values of the angular momentum as can occur experimentally, then equation 5.1 overestimates the fusion cross section as it assumes that all of the reaction strength lies in the fusion channel.

We begin by discussing fusion in the light systems, where by far the greatest number of calculations have been effected. In Figure 5.1 the fusion cross section calculated[37] in the axially symmetric approximation is compared with the results of experiment for the reactions $^{12}C + ^{16}O$ [38] and $^{12}C + ^{18}O$.[39] The calculations

are in good agreement with experiment except for the most energetic point of each calculation, and for the fact that the fluctuations in the experimental cross section of the $^{12}C + ^{16}O$ system are not reproduced. It could not be determined in this calculation whether the latter defect is due to the determinantal nature of the TDHF wave function or to the filling approximation which was employed, and which masks the shell structure presumably responsible for the fluctuations.

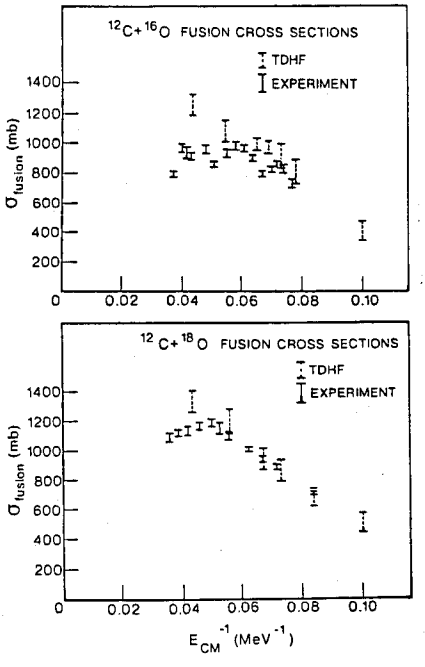

Fig. 5.1 Comparison of fusion excitation functions with experimental results.[37]

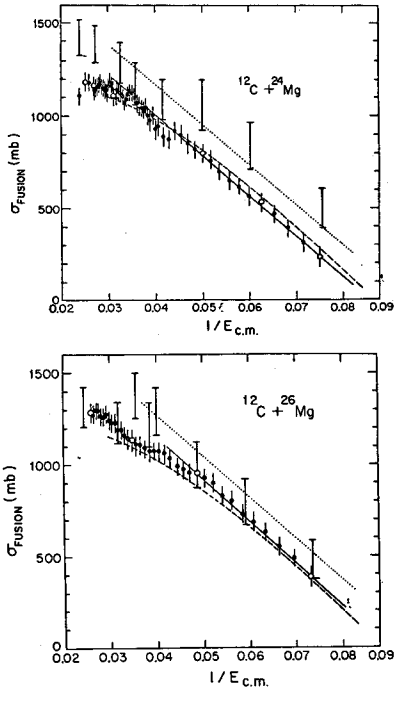

Fig. 5.2 Comparison of fusion excitation functions with experimental results.[40]

In order to clarify the above point a comparison has been made of the calculated and experimental cross sections for the systems $^{12}C + ^{24}Mg$ and $^{12}C + ^{26}Mg$.[40] In these calculations the open-shell nuclei are treated by introducing a residual pairing interaction within the constant G model.[41] Even so, the fluctuations in the experimental cross section in the alpha-like system $^{12}C + ^{24}Mg$ are not reproduced by the calculations. Referring to Figure 5.2, it may be additionally observed that the calculated cross sections consistently exceed the experimental values. As the geometry utilized in the calculation, that of an oblate carbon nucleus incident upon a prolate magnesium nucleus, tends to yield a result lower than that expected from a correct averaging over relative orientation, this difference is presumably real, and worthy of further study. The fact that the calculations do not reproduce the fluctuations should not be regarded as surprising. For the resonant structure may be traced to the alpha evaporation

channels, and the TDHF calculations which, at best, reproduce the average behavior of the system, are not expected to fit structure due to specific exit channels.

The dependence of the cross section on the parameters of the Skyrme interaction is illustrated in Figure 5.3 for the reaction $^{16}O + ^{24}Mg$. While the TDHF

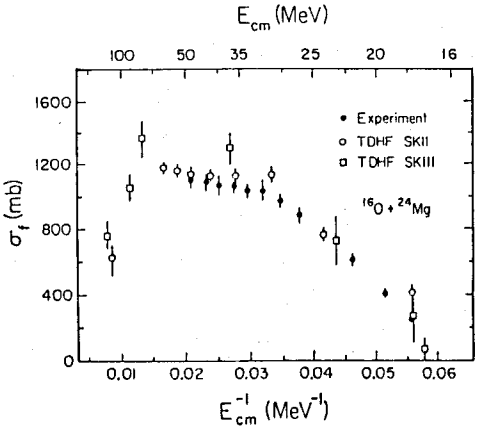

Fig. 5.3 Comparison of fusion excitation functions calculated using the interactions Skyrme II and Skyrme III with experiment.[44]

results obtained[42] using the interaction Skyrme II are in good agreement with experiment,[43] the results with Skyrme III exceed the experimental results by some 15-20% at intermediate energies.[44] The underlying reason for this enhancement has not been understood, and is of some importance, as the interaction Skyrme III, with its effective mass ratio $m^*/m = 0.76$ in nuclear matter, is the generally favored interaction.

The precipitous drop in the calculated cross section at the high energy end of the spectrum is due to the opening of an angular momentum window for fusion. Above the energy $E_{cm} \simeq 70$ MeV low angular momentum collisions result in inelastic scattering, rather than fusion. As illustrated in Figure 5.4, the minimum angular

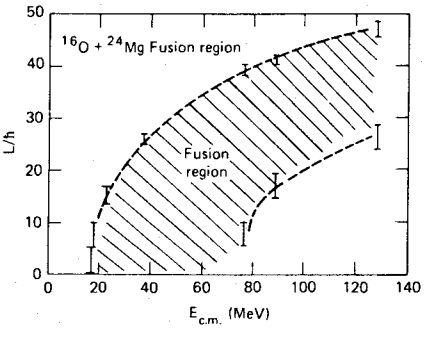

Fig. 5.4 Fusion region in the angular momentum-energy plane as calculated using the interaction Skyrme III.[44]

momentum for which fusion occurs is an increasing function of energy above the threshold of 70 MeV. This effect which has previously been observed in TDHF calculations for the systems $^{16}O + ^{40}Ca$ and $^{28}Si + ^{28}Si$,[45] $^{86}Kr + ^{139}La$ and $^{84}Kr + ^{209}Bi$[46] as well as in the present system[42),44)] remains an experimentally unverified prediction of the theory. Although experiments have been undertaken in order to observe the additional deep inelastic scattering cross section due to the non-fusion events they have not truly been conclusive. For example, the most recent experiment reported[47] an experimental upper limit of 6 mb deep inelastic for the system $^{16}O + ^{16}O$ at E_{lab} = 68 MeV, whereas TDHF calculations as cited by Davies et al.[17] give a value of 132 mb. While at first sight the difference between experiment and theory might seem sufficient to negate the theory, it must be noted that the energy 68 MeV is very close to the low energy threshold for the effect, which itself is a very sensitive function of the symmetries enforced and interactions used in the calculations.[24),46)]

The effect that the imposition of symmetries can have is illustrated in Figure 5.5 where the $^{40}Ca + ^{40}Ca$ fusion cross section is plotted as a function of

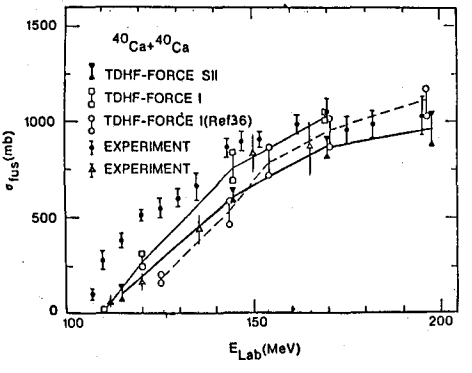

Fig. 5.5 Fusion cross section for $^{40}Ca + ^{40}Ca$.[24] See text.

energy for several calculations. To be compared are the axially symmetric calculations[24] labeled by the open squares in which isospin symmetry is <u>not</u> enforced, and the three dimensional calculations, labeled by the open circles, in which isospin symmetry <u>is</u> enforced. It may be observed that the relaxation of the isospin symmetry results in an increase of ≈200 mb at the lower energies studied. Indeed, this figure represents a lower estimate, as the axial approximation is known[28] to underestimate the fusion cross section. In general, the relaxation of any symmetry has resulted in an increase in the calculated fusion cross section, and it will be of interest to examine the effect of removing the spin degeneracy through the introduction of the spin-orbit interaction as calculated with the

improved algorithm.[25] The difference in cross section as calculated with the interactions Skyrme I and Skyrme II is presumably due to the fact that the rms radius and 10% - 90% surface thickness of ^{40}Ca are 1% and 10% less respectively calculated with Skyrme II as compared with Skyrme I.

Of particular interest is the comparison of theory with experiment. The experimental results depicted by the black circles[47] were completed prior to the TDHF calculations, and are in clear disagreement with the TDHF results at the lower energies. However the experiment recently has been repeated by two groups[48),49] whose results are in agreement with one another but not with the results of reference 47. The results of reference 49, indicated by the open triangles, are in excellent agreement with the theoretical results.

As the dominant process in the collision of heavy systems is deep inelastic scattering, with fusion contributing perhaps 1/10 of the total reaction cross section, it is an open question as to whether or not TDHF calculations can yield valid information concerning fusion in heavy systems. While much more work must be done in order to answer this question, the results of calculations effected to date are certainly not discouraging. We exemplify the fusion behavior found in such systems with a discussion of head-on collisions of ^{86}Kr + ^{139}La.

The first striking feature observed is the existence of an energy threshold for fusion. Unlike the situation in light systems, in which fusion occurs at an energy immediately above the Coulomb barrier, in heavy systems it is found[46] that there exists an energy region above the barrier below which fusion does not occur. In this region very long collision times are observed and the system develops a pronounced neck reminiscent of a molecular configuration. At higher energies fusion is observed over a broad range ≈200 MeV. Although the fusion cross sections calculated[46] using the interaction Skyrme II are in considerable disagreement with the available experimental results the defect may well be in the interaction rather than the calculation. Indeed, calculation with the interaction Skyrme III shows that there exists a 150 MeV difference in the fusion threshold as compared to that obtained using Skyrme II. As shown in Table 5.1, reproduced from

Table 5.1

E_{lab} (MeV)	σ_f(expt.) (mb)	σ_f(axi. sym) Skyrme II	σ_f(sep.) Skyrme III
505	170±50	no fusion	201±55
610	225±50	no fusion	
710	170±50	141±20	89±15

Davies et al,[17] the Skyrme III results are in reasonable agreement with experiment.

To illustrate the deep inelastic processes, as calculated in TDHF, we compare the calculated cm energies and scattering angles with the experimental Wilczynski plot as given in Davies et al.[17] for the $^{86}Kr + ^{139}La$ system. As may be seen in Figure 5.6, the experimental energy losses and scattering angles are fairly well produced in the grazing, and quasi-elastic regions, although the low angular momentum points lie approximately 50 MeV above the experimental ridge. At 710 MeV, the calculations are in similar agreement. However at 505 MeV, the calculated points have too little dissipation and are not sufficiently forward in angle.

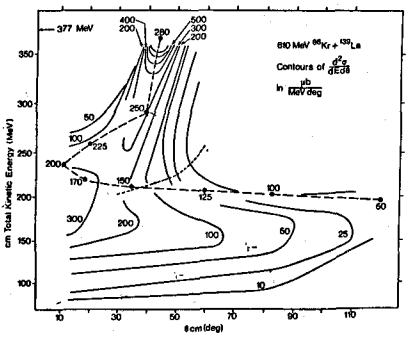

Fig. 5.6 Comparison of calculated points labeled by the initial L with the experimental Wilczynski plot.[17]

Other observables which can be compared with experiment include the charge and mass distribution widths. Although the TDHF widths are always much smaller than the experimental widths, such comparisons represent overly stringent tests of the mean-field theory, since they require the evaluation of two-body matrix elements.

6. SUMMARY

The domains of validity of the various approximations to full three-dimensional TDHF calculations are fairly well understood at this point. Further work needs to be done to determine the appropriate effective interaction to employ, and it is important to investigate the effects of relaxing the spin symmetry. Nevertheless significant progress has been made in effecting realistic calculations, and comparison with experiment, especially for fusion in light systems, where most of the data exists, is extremely encouraging. Finally, it is important that better calculations, as well as experiments at higher energy be effected in order to settle the question as to the existence or non-existence of an angular momentum window for fusion.

REFERENCES

1. P.A.M. Dirac, Proc. Camb. Phil. Soc. 26, 376 (1930).
2. P. Bonche, S. E. Koonin, and J. W. Negele, Phys. Rev. C13, 1226 (1976).
3. G. Wegmann, Physics Lett. 50B, 327 (1974); S. E. Koonin, Prog. in Part. and Nucl. Phys. 4, 283 (1980).
4. J. A. Wheeler, Phys. Rev. 52, 1083, 1107 (1937).
5. D. L. Hill and J. A. Wheeler, Phys. Rev. 89, 1102 (1953).
6. A. de-Shalit and H. Feshbach, Theoretical Nuclear Physics, (Wiley, New York, 1974) Vol. 1, p. 541.
7. S. T. Belyaev, Nucl. Phys. 64, 17 (1965); F. M. H. Villars, in Dynamic Structure of Nuclear States, Proceedings of the 1971 Mont Tremblant International Summer School, edited by D. J. Rowe (Univ. of Toronto Press, Toronto, 1972); M. Baranger and M. Veneroni, Ann. Phys. (N.Y.) 114, 123 (1978).
8. K. T. R. Davies, A. J. Sierk, and J. R. Nix, Phys. Rev. C6, 2385 (1976).
9. Y. M. Engel, D. M. Brink, K. Goeke, S. J. Krieger, and D. Vautherin, Nucl. Phys. A249, 215 (1975).
10. S. J. Krieger and K. Goeke, Nucl. Phys. A234, 269 (1974).
11. S. E. Koonin, Ph.D. thesis, Massachusetts Institute of Technology, 1975 (unpublished); C. Y. Wong, J. A. Maruhn, and T. A. Welton, Nucl. Phys. A256, 469 (1975).
12. S. Levit, Phys. Rev. C21, 1594 (1980); S. Levit, J. W. Negele, and Z. Paltiel, Phys. Rev. C21, 1603 (1980); Y. Alhassid, B. Müller, and S. E. Koonin, Phys. Rev. C23, 487 (1981).
13. Y. Alhassid and S. E. Koonin, Phys. Rev. C23, 1590 (1981).
14. J. W. Negele, in Proceedings of the Meeting on Heavy Ion Collisions, Fall Creek Falls State Park, Pikeville, Tennessee (1977); P. C. Lichtner and J. J. Griffin, Phys. Rev. Lett. 37, 1521 (1976).
15. A. Kerman and S. E. Koonin, Ann. Phys. 100, 332 (1976).
16. G. E. Brown, Unified Theory of Nuclear Models (North-Holland, Amsterdam, 1964).
17. J. W. Negele in Theoretical Methods in Medium Energy and Heavy-Ion Physics, K. McVoy and W. A. Friedman, ed. (Plenum Press, New York, 1978); S. E. Koonin, Progress in Part. and Nucl. Phys. 4, 283 (1980); J. W. Negele (to be published in Reviews of Modern Physics); K. T. R. Davies, K. R. S. Devi, S. E. Koonin and M. R. Strayer, Cal-Tech preprint MAP-23 (1982).
18. R. Y. Cusson, H. P. Trivedi, H. W. Meldner R. Wright and M. S. Weiss, Phys. Rev. C14, 1615 (1976).
19. T. H. R. Skyrme, Phil. Mag. 1, 1043 (1956); Nucl. Phys. 9, 615 (1959).
20. P. Quentin and H. Flocard, Ann. Rev. of Nuc. and Part. Science 28, 523 (1978).
21. J. W. Negele and D. Vautherin, Phys. Rev. C5, 1472 (1973).

22. J. W. Negele, Phys. Rev. C1, 1260 (1970).
23. P. Hoodbhoy and J. W. Negele, Nucl. Phys. A288, 23 (1977).
24. S. J. Krieger and K. T. R. Davies, Phys. Rev. C18, 2567 (1978).
25. P. H. Heenen, private communication.
26. J. A. Maruhn and R. Y. Cusson, Nucl. Phys. A270, 471 (1976); R. Y. Cusson and J. A. Maruhn, Phys. Letts. B62, 134 (1976).
27. S. E. Koonin, K. T. R. Davies, V. Maruhn-Rezwani, H. Feldmeier, S. J. Krieger, and J. W. Negele, Phys. Rev. C15, 1359 (1977).
28. K. T. R. Davies, H. T. Feldmeier, H. Flocard, and M. S. Weiss, Phys. Rev. C18, 2631 (1978).
29. H. T. Feldmeier, ORNL Report ORNL/TN6053 (1977).
30. K. R. Sandhya Devi and M. R. Strayer, Phys. Letts. B77, 135 (1978).
31. S. E. Koonin, B. Flanders, H. Flocard, and M. S. Weiss, Phys. Letts., B77, 13, (1978).
32. In the filling approximation, a spherical nucleus is constructed by assigning equal, time-independent fractional occupation probabilities, n_i to the orbitals of the last shell. Although the density $\rho = \Sigma_j \; n_j \psi_j \psi_j^*$ then no longer satisfies the HF condition $\rho^2 = \rho$, this technique has been adopted in order to obtain spherically symmetric solutions for open-shell nuclei.
33. K. R. Sandhya Devi, M. R. Strayer, K. T. R. Davies, S. E. Koonin, and A. K. Dhar (to be published in Phys. Rev. C).
34. E. Tomasi, D. Ardouin, J. Barreto, V. Bernard, B. Cauvin, C. Magnago, C. Mazur, C. Ngô, E. Piasecki, and M. Ribrag, Nucl. Phys. A373, 341 (1982).
35. M. Lefort, Rep. Prog. Phys. 39, 129 (1976).
36. P. Bonche, B. Grammaticos, and S. E. Koonin, Phys. Rev. C17, 1700 (1978).
37. S. J. Krieger and K. T. R. Davies, Phys. Rev. C20, 167 (1979).
38. P. Sperr, S. Vigdor, Y. Eisen, W. Henning, D. G. Kovar, T. R. Ophel, and B. Zeidman, Phys. Rev. Lett. 36, 405 (1976).
39. P. Sperr, T. H. Braid, Y. Eisen, D. G. Kovar, F. W. Prosser, Jr., J. P. Schiffer, S. L. Tabor, and S. Vigdor, Phys. Rev. Lett. 37, 321 (1976).
40. K. Daneshvar, D. G. Kovar, S. J. Krieger, and K. T. R. Davies, Phys. Rev. C25, 1342 (1982).
41. J. Blocki and H. Flocard, Nucl. Phys. A273, 45 (1976).
42. K. R. S. Devi, A. K. Dhar, and M. R. Strayer, Phys. Rev. C23, 2062 (1981).
43. S. Tabor, D. Geesaman, W. Henning, D. Kovar, K. Rehn, and F. Prosser, Phys. Rev. C17, 2136 (1978).
44. S. J. Krieger and M. S. Weiss, Phys. Rev. C24, 928 (1981).
45. P. Bonche, K. T. R. Davies, B. Flanders, H. Flocard, B. Grammaticos, S. E. Koonin, S. J. Krieger, and M. S. Weiss, Phys. Rev. C20, 641 (1979).
46. K. T. R. Davies, K. R. Sandhya Devi, and M. R. Strayer, Phys. Rev. C24, 2576 (1981).

47. A. Lazzarini, H. Doubre, K. T. Lesko, V. Metag, A. Seamster, R. Vandenbosch, and W. Merryfield, Phys. Rev. C24, 309 (1981).

48. J. Barreto, G. Auger, H. Doubre, M. Langevin, and E. Plagnol, Annual Report IPN Orsay (1980) to be published.

49. E. Tomasi, D. Ardouin, J. Barreto, V. Bernard, B. Cauvin, C. Magnago, C. Mazur, C. Ngô, E. Piasecki, and M. Ribrag, Nucl. Phys. A373, 341 (1982).